Synthesis, Characterization, DFT, and Thermogravimetric Analysis of Neutral Co(II)/Pyrazole Complex, Catalytic Activity toward Catecholase and Phenoxazinone Oxidation

Mohamed El Boutaybi, Nadia Bouroumane, Mohamed Azzouzi, Mohamed Aaddouz, Said Bacroume, Mohamed El Miz, Rachid Touzani, Zahra Bahari, Abdelkader Zarrouk, Adel El-Marghany, et al.

crystals

MDPI

Article

Synthesis, Characterization, DFT, and Thermogravimetric Analysis of Neutral Co(II)/Pyrazole Complex, Catalytic Activity toward Catecholase and Phenoxazinone Oxidation

Mohamed El Boutaybi [1,*], Nadia Bouroumane [1], Mohamed Azzouzi [1], Mohamed Aaddouz [2], Said Bacroume [3], Mohamed El Miz [1], Rachid Touzani [3], Zahra Bahari [1], Abdelkader Zarrouk [4], Adel El-Marghany [5], Charafeddine Jama [6], Ahmed Abu-Rayyan [7] and Ismail Warad [8,*]

1 Multidisciplinary Faculty of Nador, Laboratory of Molecular Chemistry, Materials and Environment (LMCME), University Mohammed Premier, Oujda 60000, Morocco
2 Faculty of Sciences, Laboratory of Environment and Applied Chemistry (LCAE), University Mohammed Premier, Oujda 60000, Morocco
3 Superior School of Technology, Laboratory of Applied Mathematics and Information Systems (LAMIS), University Mohammed Premier, Nador 60000, Morocco
4 Laboratory of Materials, Nanotechnology, and Environment, Faculty of Sciences, Mohammed V University in Rabat, Agdal-Rabat P.O. Box 1014, Morocco
5 Department of Chemistry, College of Science, King Saud University, P.O. Box 2455, Riyadh 11451, Saudi Arabia
6 UMR 8207—UMET—Unité Matériaux et Transformations, Centrale Lille, INRAE, CNRS, University Lille, 59000 Lille, France
7 Chemistry Department, Faculty of Arts & Science, Applied Science Private University, P.O. Box 166, Amman 11931, Jordan
8 Department of Chemistry, AN-Najah National University, Nablus P.O. Box 7, Palestine
* Correspondence: m.elboutaybi@ump.ac.ma (M.E.B.); warad@najah.edu (I.W.)

Citation: Boutaybi, M.E.; Bouroumane, N.; Azzouzi, M.; Aaddouz, M.; Bacroume, S.; El Miz, M.; Touzani, R.; Bahari, Z.; Zarrouk, A.; El-Marghany, A.; et al. Synthesis, Characterization, DFT, and Thermogravimetric Analysis of Neutral Co(II)/Pyrazole Complex, Catalytic Activity toward Catecholase and Phenoxazinone Oxidation. *Crystals* **2023**, *13*, 155. https://doi.org/10.3390/cryst13020155

Academic Editor: Kil Sik Min

Received: 25 December 2022
Revised: 9 January 2023
Accepted: 11 January 2023
Published: 17 January 2023

Abstract: The pyrazole-pyridin-2-amine, as a tridentate pyrazole ligand, and its neutral Co(II)/pyrazole complex were prepared using a direct method with a high yield. The desired pyrazole ligand and its complex were subjected to several physicochemical and thermal analyses; moreover, the DFT-like optimization of MEP, HOMO/LUMO, and TD-DFT correlated well with their experimental relatives. Additionally, the oxidation catalytic activities of the Co(II)/pyrazole complex, such as the catecholase of catechol to o-quinone and the phenoxazinone of 2-aminophenol to 2-aminophenoxazinone, were also evaluated under mild RT conditions and atmospheric oxygen.

Keywords: cobalt(II); pyrazole; catecholase; phenoxazinone; DFT

1. Introduction

The pyrazoles, as N-donor compounds, have been inclusively matured as chelate ligands for metal ions' coordination [1]. N-pyrazole derivative ligands and their complexes are used because of their stability, catalytic coordination abilities and versatility [1,2]. In particular, Co(II)/pyrazole complexes have received attention in several applications, where most researchers are using these complexes as catalysts, with an eye on their promising medical role [3–7].

Catalysis has long been the main field of chemistry in several technological, pharmaceutical and medicinal fields [8,9]. Among the catalysts studied are enzymes, which are organic substances, produced by living cells. A number of these enzymes are able to catalyze the activation of atmospheric oxygen in a variety of reactions [10]. One of these enzymes is catechol oxidase [10,11] (copper enzyme), which catalyzes the aerobic oxidation of diphenols to o-quinone [12,13].

Catechol compounds are abundant in nature. They are used with different neurotransmission functions [14,15], and their surface adhesion and crosslinking of catecholamine proteins has been the subject of several catalytic studies, including some with the goal to develop biomimetic catalysis of the oxidation of catechol to o-quinone [16–18].

Quinones are ubiquitous compounds in nature and one of the essential elements in living organisms. They are particularly involved in the cellular respiratory chain to transport electrons [11].

The efficiency and selectivity of Cu(II)-metalloenzymes in catechol oxidation have recently been developed to enhance the catalytic and structural properties of such enzymes [19,20].

For the first time, a novel Co(II)/pyrazole complex has been prepared with sufficient yield. Several physicochemical analyses were performed on the Co(II)/pyrazole complex, and the results were successfully compared to their DFT theoretical counterparts. Under mild conditions, the desired complex demonstrated a high degree of catalytic activity of metalloenzyme catechol to o-quinone and aminophenol to phenoxazinone oxidase.

2. Materials and Methods

2.1. Materials

All materials were purchased from Sigma-Aldrich, USA, and used as received without further purification, except for 1-hydroxymethyl-3,5-dimethylpyrazole, which was synthesized. The materials used in this study were acetonitrile, methanol, tetrahydrofuran, 1-hydroxymethyl-3,5-dimethylpyrazole, 5-chloropyridin-2-amine, dihydroxy-1,2-benzene (catechol), magnesium sulfate, dichloromethane and metal salt ($CoCl_2$, $6H_2O$).

Several characterization methods were used on the prepared ligand and its complex, such as Fourier transform infrared (FTIR) supported by pressed KBr pellets (4500–400 cm^{-1}); nuclear magnetic resonance (NMR) spectra were recorded on a Bruker-400 operating at 400 MHz for 1H spectra and on a UV-Vis UV 1800 PC Shimadzo spectrometer operating at 101 MHz for ^{13}C spectra; TGA and DTA were determined by utilizing DTG-60; and X-ray diffraction results were obtained using an XRD-6000 X-ray diffractometer (Shimadzu, Tokyo, Japan).

2.2. Synthesis of Tridentate Pyrazole Ligand

In a flask fitted with a magnetic stirrer, one equivalent of 1-hydroxymethyl-3,5-dimethylpyrazole (5 g) in 40 mL of acetonitrile was mixed with one equivalent of 5-chloropyridin-2-amine in 20 mL of acetonitrile (Scheme 1). The reaction was stirred at room temperature for 120 h, and then the mixture was dried over $MgSO_4$, filtered and concentrated with a rotavapor and purified by CH_2Cl_2/H_2O extraction [21–23].

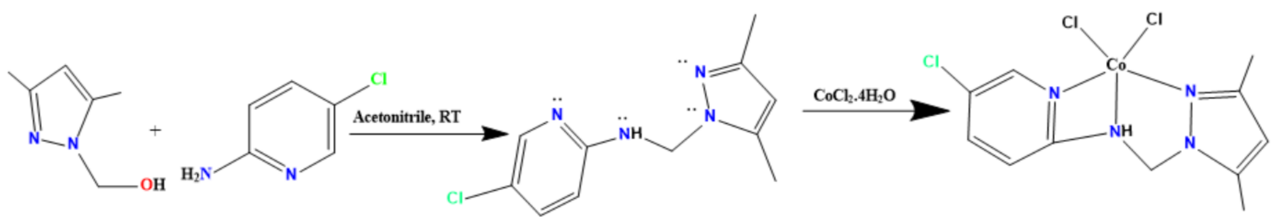

Scheme 1. Preparation of tridentate pyrazole ligand and its Co(II) complex.

2.3. DFT Calculations

All species in this work were optimized using the MN15L Minnesota functional [24] and the 6-31+G(d,p) basis set. The MN15L functional performed excellently in describing similar systems in previous works [25–28]. Frequency calculations were performed following the optimization to ensure the expected frequencies were found. The Co configuration in the complex was found to have a square pyramidal structure with a spin multiplicity of 2 (doublet). Therefore, unrestricted SCF was used by adding the prefix –u to the Gaussian input. The molecular orbitals of the complex were probed as previously described [25,29,30]. All calculations were carried out using Gaussian 16 Rev C.01 [31] and viewed using GaussView [32].

2.4. Synthesis of Co(II)/Pyrazole Complex

The methanolic solution (5 mL) of $CoCl_2.6H_2O$ (49.965 mg, 0.21 mmol) was added to CH_3CN solution (10 mL) of 5-chloro-N-((3,5-dimethyl-1H-pyrazol-1-yl)methyl)pyridin-2-amine (50 mg, 0.21 mmol). A product in blue solution was filtered to remove the solid impurities and then left to evaporate at room temperature. After almost a week, a blue powder of Co(II)/pyrazole was formed.

2.5. Catecholase Studies

The experiments were carried out in methanol under ambient conditions on a UV-Vis UV 1800 PC Shimadzo spectrometer (Multidisciplinary Faculty of Nador). The measurement of the absorbance of o-quinone over time (from 0 to 65 min) followed at 390 nm. Before that, to prepare the complex formed in situ, we mixed successively 0.15 mL of a solution (2×10^{-3} mol/L) of the metal with 0.15 mL of a solution of the ligand (2×10^{-3} mol/L) or 0.3 mL of the solution of the prepared complex (2×10^{-3} mol/L). Afterward, we added 2 mL of the catechol solution with a concentration of 10^{-1} mol/L. We have discussed three oxidative transformations in this article (Scheme 1): catecholase, tyrosinase and oxidation of 2-aminophenol.

3. Results

3.1. Synthesis, EDX, PXRD and DFT-Optimization

Mixing 1-hydroxymethyl-3,5-dimethylpyrazole with 4-chloropyridin-2-amine under vigorous stirring for 5 days in acetonitrile empowered the formation of the tridentate pyrazole ligand at a high yield and with water as the only bi-product, as can be seen in Scheme 2. One equivalent of the synthesized ligand was treated with $CoCl_2{\cdot}4H_2O$, resulting in a spontaneous green color appearing. Such a change in the color strongly supported the tri-chelate of the ligand via the 3N coordinated Co(II) center to form the square pyramidal Co(II)/pyrazole complex, as can be seen in Scheme 1.

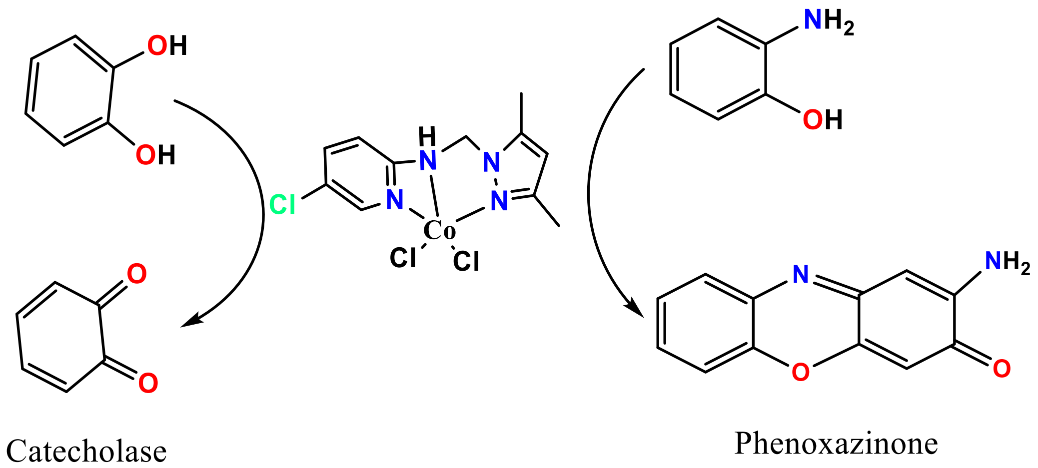

Scheme 2. Catalyzed catecholase and phenoxazinone processes.

To confirm the presence of five coordination bonds around the Co(II) center in the absence of XRD-crystal and NMR measurements, Job's method of titration was applied. The UV-Vis Job's method produced a one-to-one metal-to-ligand stochiometric ratio, which supported the presence of the expected 5 coordination structure since the ligand is considered to be tridentate. Additionally, several publications that have recently succeeded in resolving the XRD structures of similar complexes were used to support our assessment of whether the expected structure could be found [33–36]. To support the purity of the desired

Co(II) complex, energy-dispersive X-ray (EDX) and PXRD analyses were performed, as can be seen in Figure 1. EDX (Figure 1a) reflected the presence of only five types of atoms in the complex backbone, while the presence of a Co center was confirmed by energy signals at 0.8, 6.9 and 7.6 KeV. Meanwhile, the C, N and Cl atoms appeared at signals with 0.1, 0.25 and 2.5 KeV positions, respectively, as can be seen in Figure 1a. Since the Co(II)/pyrazole complex does not crystallize to a degree suitable for XRD single crystal analysis, PXRD was performed only to check the purity and crystallinity of the complex. The percentage of sharp, long-range atomic order patterns without broad scattering band peaks supported the high purity. Moreover, all the possible diffraction peaks were observed, leading us to surmise that the Co(II)/pyrazole complex is a polycrystalline type containing thousands of crystallite systems with different ratios, but with a monoclinic predominant lattice, as can be seen in Figure 1b.

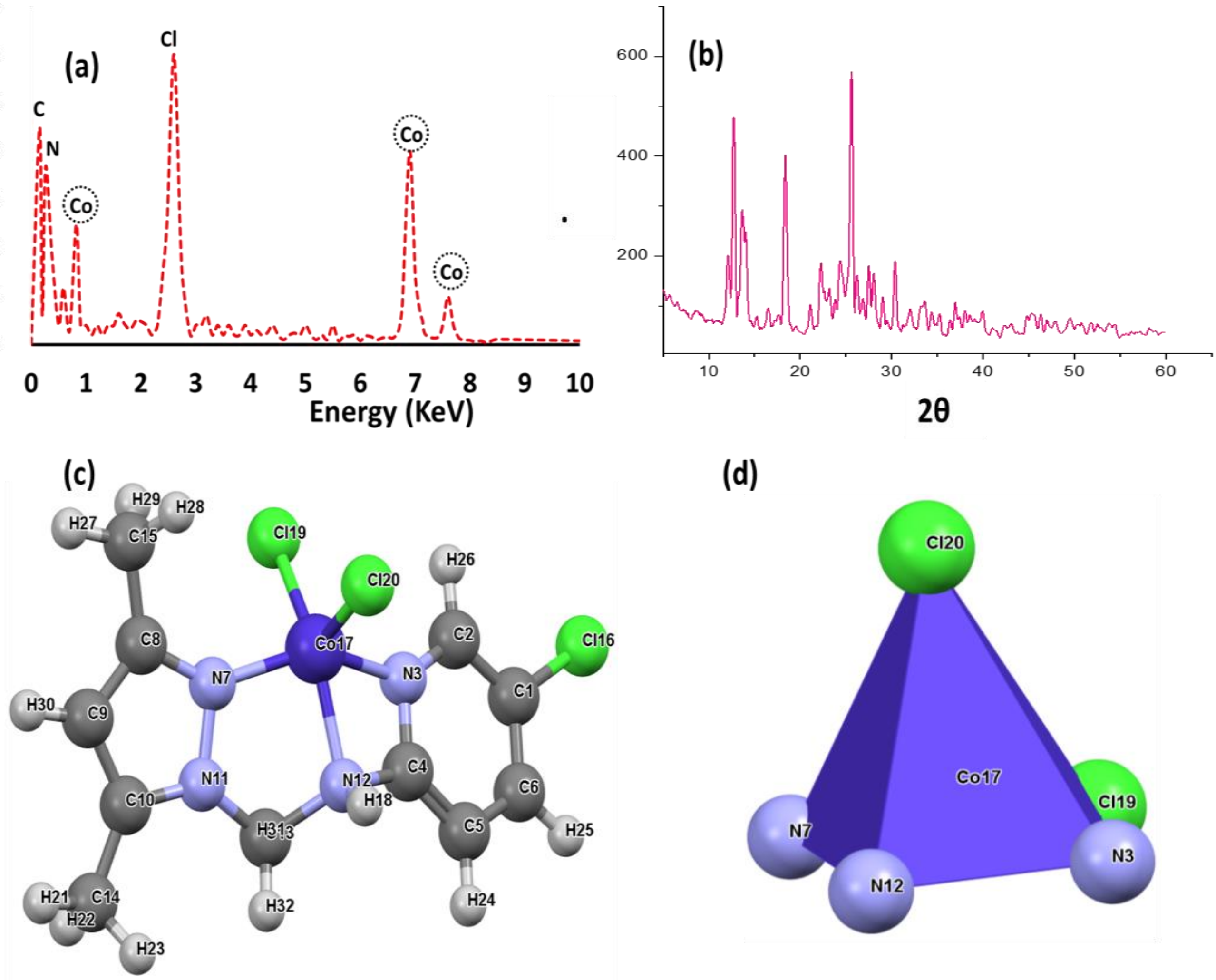

Figure 1. (**a**) EDX analysis of the Co(II)/pyrazole complex, (**b**) PXRD spectra of cobalt complex, (**c**) DFT-optimization and (**d**) geometry.

To acquire more knowledge about the structure around the Co(II) center in the desired neutral Co(II)/pyrazole complex, DFT-optimization was carried out. The molecular structure, together with the structural parameter, are illustrated in Figure 1c and Table 1. The DFT reflected a Co(II)/pyrazole complex with a square pyramid geometry favored over a trigonal bipyramid geometry, as can be seen in Figure 1d. Moreover, the square pyramid was found to be slightly distorted, with a dihedral angle of N7-N12-N3-Cl19 = 2.8°, as shown in Figure 1d. The angles and the bond lengths around the Co(II) were found to have the expected values, as can be seen in Table 1.

Table 1. DFT structural parameters.

No.	Bond		Å	No.	Angle			(°)	No.	Angle			(°)
1	C1	C2	1.3985	1	C2	C1	C6	120.7	23	N7	N11	C10	109.57
2	C1	C6	1.3967	2	C2	C1	Cl16	118.76	24	N7	N11	C13	114.48
3	C1	Cl16	1.7782	3	C6	C1	Cl16	120.54	25	C10	N11	C13	134.35
4	C2	N3	1.3432	4	C1	C2	N3	117.93	26	C4	N12	C13	120.26
5	N3	C4	1.3579	5	C2	N3	C4	121.96	27	C4	N12	Co17	89.11
6	N3	Co17	1.9101	6	C2	N3	Co17	141.77	28	C13	N12	Co17	105.77
7	C4	C5	1.3717	7	C4	N3	Co17	96.24	29	N11	C13	N12	103.1
8	C4	N12	1.4737	8	N3	C4	C5	122.93	30	N3	Co17	N7	141.71
9	C5	C6	1.4084	9	N3	C4	N12	104.6	31	N3	Co17	N12	70.04
10	N7	C8	1.3819	10	C5	C4	N12	132.46	32	N3	Co17	Cl19	89.87
11	N7	N11	1.4364	11	C4	C5	C6	116.5	33	N3	Co17	Cl20	108.4
12	N7	Co17	1.8122	12	C1	C6	C5	119.98	34	N7	Co17	N12	85.79
13	C8	C9	1.3949	13	C8	N7	N11	106.46	35	N7	Co17	Cl19	93.17
14	C8	C15	1.4899	14	C8	N7	Co17	139.58	36	N7	Co17	Cl20	105.99
15	C9	C10	1.4108	15	N11	N7	Co17	113.06	37	N12	Co17	Cl19	143.67
16	C10	N11	1.3608	16	N7	C8	C9	108.13	38	N12	Co17	Cl20	104.09
17	C10	C14	1.49	17	N7	C8	C15	123.31	39	Cl19	Co17	Cl20	111.03
18	N11	C13	1.4638	18	C9	C8	C15	128.51					
19	N12	C13	1.5166	19	C8	C9	C10	109.06					
20	N12	Co17	1.994	20	C9	C10	N11	106.71					
21	Co17	Cl19	2.2143	21	C9	C10	C14	128.81					
22	Co17	Cl20	2.2204	22	N11	C10	C14	124.45					

3.2. IR Analysis

The infrared spectra of the synthesized ligand, together with its complex, are illustrated in Figure 2. In both ligand and complex spectra, the N–H band has been recorded. The slightly lower shift in the vibration of N–H in the complex (31,205 cm^{-1}) compared with the free ligand (3260 cm^{-1}) supported the coordination and the formation of a Co(II)–N bond. Moreover, such a bond was also supported by the evidencing of a new signal at 490 cm^{-1} [9]. The band at 1619 cm^{-1}, which corresponded to C=N of the ligand, shifted to a lower wavenumber (1602 cm^{-1}) on Co(II) coordination compared with its position in the ligand. These observations indicate the participation of the pyrazole ring in coordination with the metal ion through the nitrogen atom [16]. Moreover, all the other function groups in both the ligand and its complex were sited in their expected regions [33], as can be seen in Figure 2.

3.3. Thermal Analysis

In this study, thermal analyses with either thermogravimetric (TGA) or differential thermal (DTA) analysis were performed to evaluate the thermal stability behavior of both ligands and their complexes under a heating rate of 10 °C/min and an open atmosphere. The free ligand reflected a simple thermal behavior since the thermal decomposition is one-step in the range of 110–400 °C (Figure 3a) with T_{DTA} = 120 °C and zero mass residue (Figure 3b). Meanwhile, the complex was decomposed in three steps. The first step was de-structuring the water solvent from the lattice in the range of 70–100 °C (Figure 3a) with TDTA = 82 °C (Figure 3b). The second step was mainly the decomposition of the ligand from the Co(II)/pyrazole to produce a necked $CoCl_2$ compound in the range of 280–440 °C (Figure 3a) with TDTA = 430 °C (Figure 3b). The third step was decomposing $CoCl_2$ to cobalt oxide as a stable final product in the range of 570–665 °C (Figure 3a) with T_{DTA} = 655 °C (Figure 3b).

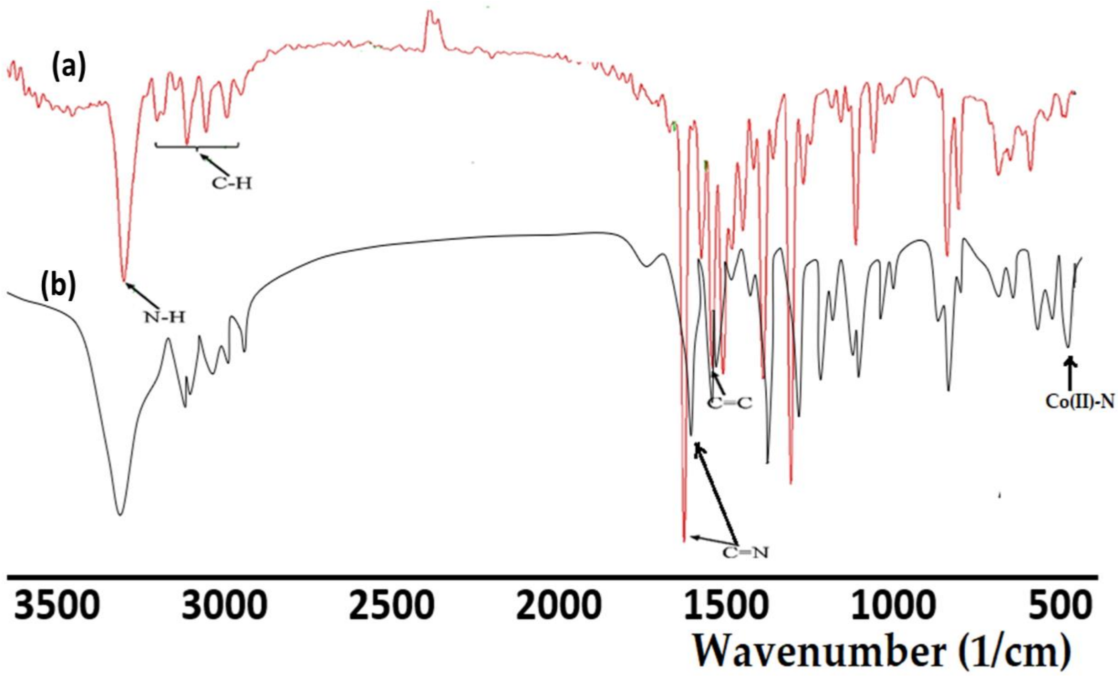

Figure 2. FTIR spectra of: (**a**) the tridentate pyrazole ligand, and (**b**) the Co(II)/pyrazole complex.

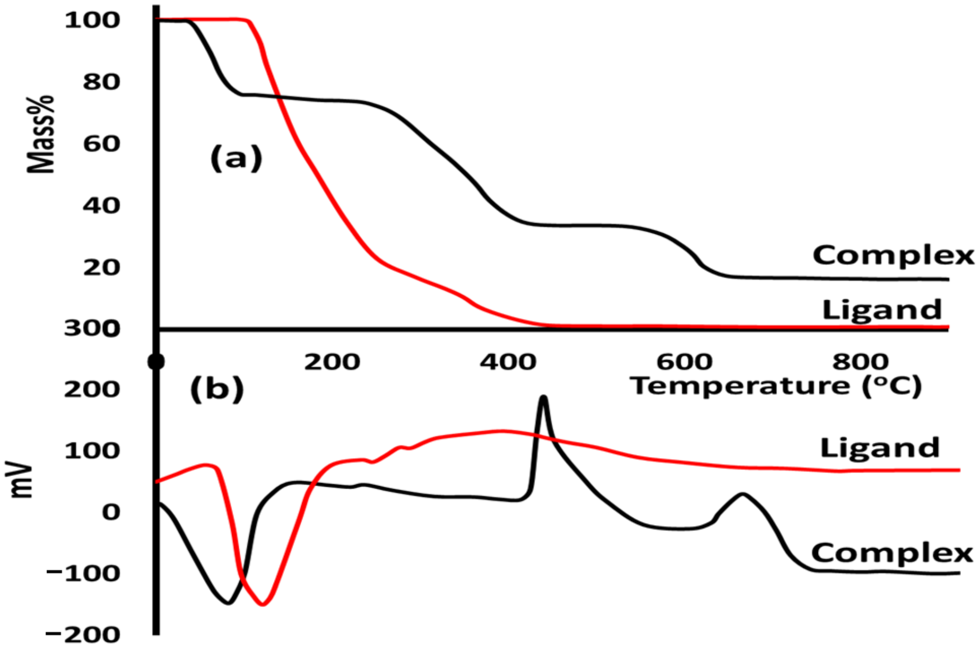

Figure 3. (**a**) TG and (**b**) DTA curves of the free ligand and its Co(II)/pyrazole.

3.4. MEP

The molecular electrostatic potential (MEP) in the range from -7.62×10^{-2} to 7.62×10^{-2} eV was used to identify electronic status sites for each of the functional groups in Co(II)/pyrazole complex 2223. The calculated electrostatic potential was obtained by using the Gaussian calculations of the prepared complex in Figure 4. The MEP showed the existence of nucleophilic, electrophilic and neutral areas, highlighted in red, blue and green colors, respectively. As expected, the chloro ligands possess a high e-rich center; meanwhile, the H of amine, H of CH_2 and H of Me proton are distinguished by their e-poor centers, and the other atoms are in a green color, denoting that they had a neutral center with a minimum value of about -7.62×10^{-2} eV. In addition, the positive region or the electron-depleted zone (blue) is located on the hydrogen atom of the aliphatic amine and the two hydrogen atoms linked to $C1_3$ with a maximum value of about 7.62 × 10^{-2} eV, and the neutral region (green) covers the rest of the molecule. Because the complex contains both electrophilic and nucleophilic sites, intermolecular forces are expected to be found with high intensity in the lattice of the complex.

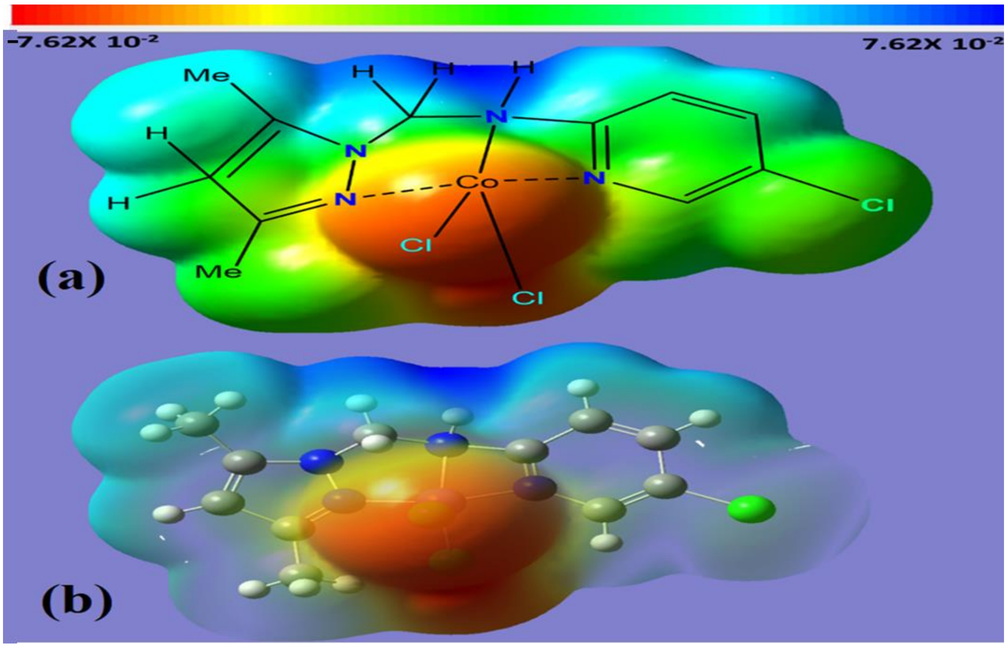

Figure 4. (**a**) Solid MEP and (**b**) transmit MEP.

3.5. HOMO/LUMO, DFT and TD-DFT

For the Co(II)/pyrazole complex, unrestricted SCF HOMO/LUMO shapes are illustrated in Figure 5a. The electronic density in HOMO was localized on the medial of the CoN_5Cl_2 complex's center more so than on the pyridine ring of the pyrazole rings, while the electronic density was found in the whole complex, meaning that the electronic situation supported the NNN ligand as a strong electron donor since it is a strong sigma donor and bi acceptor (Figure 5a).

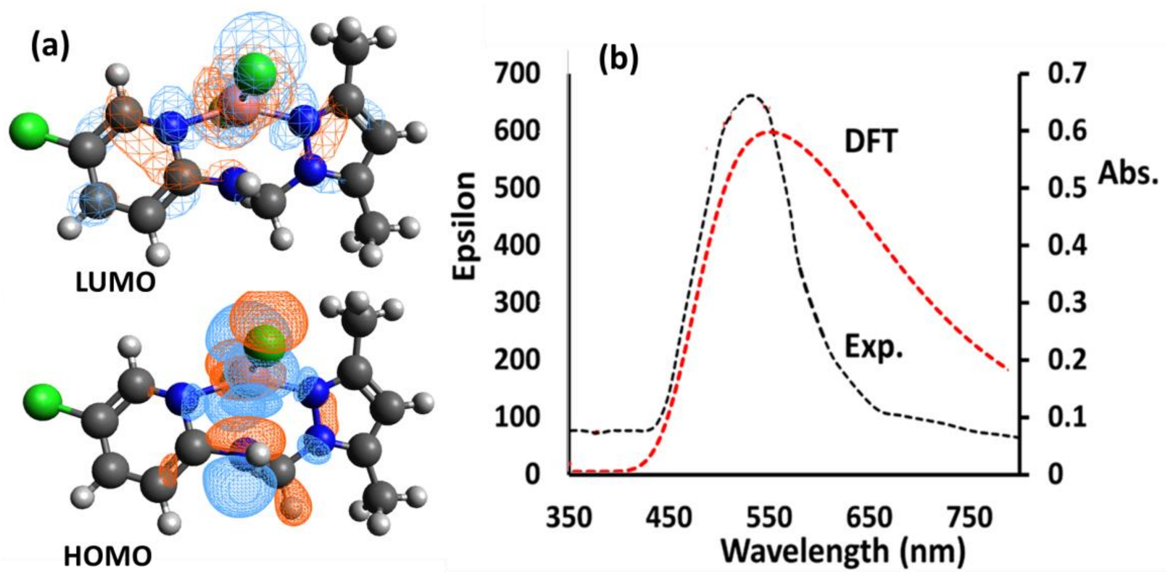

Figure 5. (**a**) HOMO/LUMO, and (**b**) visible/TD-DFT of the Co(II)/pyrazole complex in MeOH.

TD-DFT/Vis electronic behavior was theorized and compared to the experimental behavior when using MeOH as a solvent, as illustrated in Figure 5b. The electronic transfers appeared in both the UV (~200–350 nm) and the visible areas (~400–650 nm). Herein, we concentrate only on the d-to-d electron transfer band because it is visible to the naked eye. The experimental spectrum of the desired complex exhibited a sharp peak at λ_{max} = 555 nm, whereas TD-DFT exhibited broad absorption at λ_{max} = 565 nm. As shown in Figure 5b, there appears to be a high degree of congruence between the theoretical and experimental measurements. Theoretical electronic transition lines for the eight highest energy levels are represented, along with their energy values, wavelengths, oscillator strengths (f) and major contributions of orbitals. Signals with f-values less than 0.01 were excluded, as represented in Table 2.

Table 2. Main TD-DFT bands with their parameters.

No.	λ_{nm}	f	Major Contributions
1	685.1	0.024	HOMO(A)- > LUMO(A) (97%)
2	597.9	0.004	HOMO(B)- > LUMO(B) (71%)
3	562.11	0.016	H-2(A)- > LUMO(A) (25%), H-2(B)- > L + 1(B) (38%), H-1(B)- > L + 1(B) (23%)
4	501.7	0.014	H-1(B)- > LUMO(B) (74%)
5	482.2	0.013	H-2(B)- > LUMO(B) (51%), HOMO(B)- > L + 2(B) (13%), HOMO(B)- > L + 3(B) (22%)
6	472.1	0.012	H-2(B)- > LUMO(B) (32%), HOMO(B)- > L + 2(B) (13%), HOMO(B)- > L + 3(B) (39%)
7	448.3	0.011	H-1(A)- > LUMO(A) (24%), HOMO(A)- > L + 1(A) (10%), HOMO(B)- > L + 2(B) (13%), HOMO(B)- > L + 3(B) (30%)
8	432.7	0.016	HOMO(A)- > L + 1(A) (26%), H-2(B)- > L + 2(B) (39%), H-1(B)- > L + 1(B) (14%)
9	417.7	0.014	H-3(A)- > LUMO(A) (25%), H-2(B)- > L + 1(B) (26%), H-1(B)- > L + 1(B) (11%), H-1(B)- > L + 2(B) (20%)
10	365.9	0.0411	H-2(A)- > L + 1(A) (83%)

3.6. Catalytic Activity toward Catecholase and Phenoxazinone

The oxidation ability of the desired Co(II)/pyrazole complex was evaluated through the catecholase of catechol to o-quinone and the phenoxazinone of 2-aminophenol to 2-phenoxazinone, as can be seen in Scheme 2.

The processes were performed in an open O_2 atmosphere and using MeOH as solvent. The reactions were monitored by UV-Vis; the final products were isolated individually and confirmed by NMR. In both processes, no oxidation reaction or color changes were observed in the absence of the Co(II)/pyrazole complex. The reacting of 0.4 M of catechol (catecholase) and 2-aminophenol (phenoxazinone) individually in the presence of 2×10^{-3} M of Co(II)/pyrazole complex dissolved in 10 mL of MeOH (with1cat.:200 substrate) allowed both processes to be completed in no more than one hour, as can be seen in Figure 6. For catecholase, the appearance of a new single peak with λ_{max} = 390 nm supported the formation of pure o-quinone [37–41], as can be seen in Figure 6a. The process reached full complexness with >99% conversion within the first 45 min (Figure 6b); meanwhile, the appearance of new peaks with λ_{max} = 433 nm during the phenoxazinone process confirmed the formation of 2-aminophenoxazinone [38–47], as can be seen in Figure 6c; this process reached full completeness with >99% conversion after 70 min (Figure 6d). Thus, the Co(II)/pyrazole complex catalyzed the catecholase process better than the phenoxazinone process, as can be seen in Figure 6.

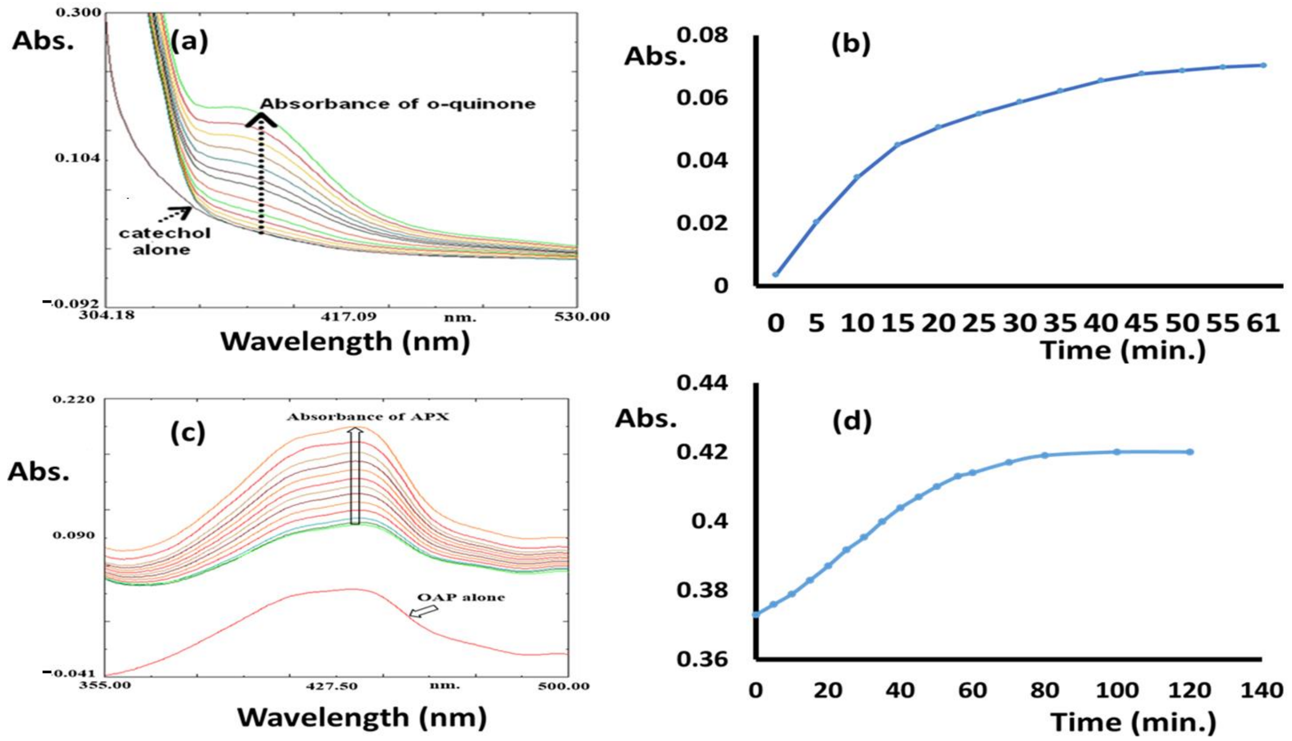

Figure 6. Co(II)/pyrazole catalytic processes: (**a**) o-quinone λ_{max} absorption (time: 5 min each run), (**b**) catecholase processing over time, (**c**) 2-phenoxazinone λmax absorption (time: 5 min each run), and (**d**) 2-phenoxazinone processing over time.

Since the Co(II)/pyrazole complex acted as a good catalyst for the catecholase process, a kinetic study of o-quinone was conducted using the initial rate method under the same catecholase condition. To obtain both Vmax and Km kinetic parameters of catecholase when catalyzed by the desired Co(II)/pyrazole complex, the Michaelis–Menten and Lineweaver−Burk models were applied, as can be seen in Figure 7a,b, respectively.

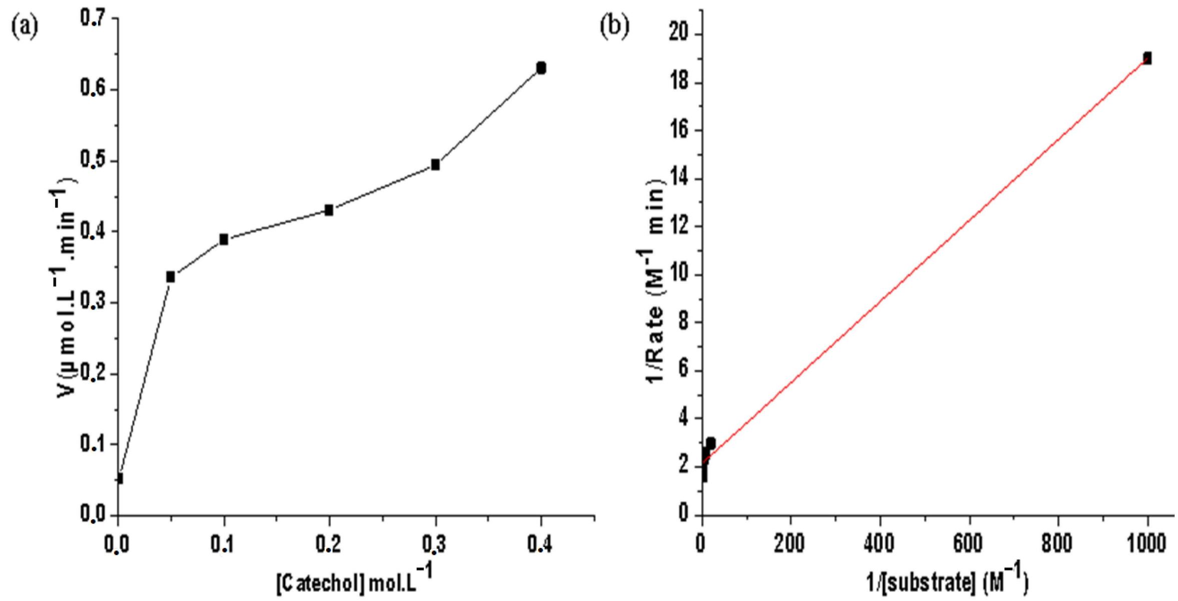

Figure 7. Co(II)/pyrazole catalyzed catecholase of o-quinone in a MeOH and open O_2-RT condition: (**a**) Michaelis–Menten correlation, and (**b**) Lineweaver−Burk plot.

The V_{max} value was found to be 0.631 μmol·L^{-1}·min^{-1} and K_m = 0.007 mol·L^{-1}. These kinetic parameters values are compatible with the results of others using similar complexes [3–11]. In addition, by comparing this with results from the literature, one can classify the desired Co(II)/pyrazole complex as working well in the catecholase process in the absence of an oxidizing agent besides atmospheric oxygen.

4. Conclusions

In conclusion, the pyrazole ligand and Co(II)/pyrazole complex were prepared by straightforward and rapid methods with high yields. The structures of the free ligand and its complex were analyzed via several physical analyses such as NMR, IR, UV-Vis. P-XRD and EDX. Additionally, DFT optimization, MEP and DFT/TD-DFT were successfully compared to their experimental values. Under mild RT open room conditions, the desired Co(II)/pyrazole complex had strong catalytic oxidation properties with the catecholase and phenoxazinone processes. Catecholase was processed with Vmax = 0.631 μmol·L^{-1}·min^{-1} and K_m = 0.007 mol·L^{-1}, showing a fast complete oxidation speed.

Author Contributions: Formal analysis, M.E.B., N.B., A.Z., M.A. (Mohamed Azzouzi) and M.A. (Mohamed Aaddouz); data curation, S.B. and M.E.M.; review and editing, R.T., A.E.-M., C.J., Z.B. and A.A.-R.; writing, I.W. All authors have read and agreed to the published version of the manuscript.

Funding: The authors extend their appreciation to the Researcher Support Project (number RSPD2023R667) of King Saud University, Riyadh, Saudi Arabia.

Data Availability Statement: The data supporting the findings of this study are available within the article.

Conflicts of Interest: The authors declare no conflict of interest.

References

1. La, M.G.; Ardizzoia, G.A. The Role of the Pyrazolate Ligand in Building Polynuclear Transition Metal Systems. *Prog. Inorg. Chem.* **1997**, *46*, 151–238.
2. Trofimenko, S. Recent Advances in Poly (Pyrazolyl) Borate (Scorpionate) Chemistry. *Chem. Rev.* **1993**, *93*, 943–980. [CrossRef]
3. Shin, S.; Ahn, S.H.; Choi, S.; Choi, S.-I.; Nayab, S.; Lee, H. Synthesis and Structural Characterization of 5-Coordinate Cobalt(II), Copper(II) and 4-Coordinate Zinc(II) Complexes Containing N′-Cyclopentyl Substituted N, N-Bispyrazolylmethylamine. *Polyhedron* **2016**, *110*, 149–156. [CrossRef]
4. Shin, S.; Ahn, S.H.; Jung, M.J.; Nayab, S.; Lee, H. Synthesis, Structure and Methyl Methacrylate Polymerization of Cobalt (II), Zinc (II) and Cadmium (II) Complexes with N, N′, N-Bidentate versus N, N′, N-Tridentate N, N′, N-Bis ((1H-Pyrazol-1-Yl) Methyl) Amines. *J. Coord. Chem.* **2016**, *69*, 2391–2402. [CrossRef]
5. Kim, D.; Kim, S.; Woo, H.Y.; Lee, H.; Lee, H. X-ray Crystal Structures and MMA Polymerization of Cadmium (II) Complexes with Bidentate Pyrazole Ligands: The Formation of Monomers or Dimers as a Function of a Methyl Substituent on the Pyrazole and Aniline Rings. *Appl. Organomet. Chem.* **2014**, *28*, 445–453. [CrossRef]
6. Yang, G. Synthesis and Crystal Structure of a Cobalt(II) Complex with Tris (1-Pyrazolylmethyl) Amine. *J. Chem. Crystallogr.* **2004**, *34*, 269–274. [CrossRef]
7. Pañella, A.; Pons, J.; García-Antón, J.; Solans, X.; Font-Bardia, M.; Ros, J. Synthesis of New Palladium (II) Compounds with Several Bidentate Nitrogen-Donor Ligands: Structural Analyses by 1H and 13C {1H} NMR Spectroscopy and Crystal Structures. *Inorganica Chim. Acta* **2006**, *359*, 2343–2349. [CrossRef]
8. Lima, M.J.; Tavares, P.B.; Silva, A.M.T.; Silva, C.G.; Faria, J.L. Selective Photocatalytic Oxidation of Benzyl Alcohol to Benzaldehyde by Using Metal-Loaded g-C3N4 Photocatalysts. *Catal. Today* **2017**, *287*, 70–77. [CrossRef]
9. Titi, A.; Shiga, T.; Oshio, H.; Touzani, R.; Hammouti, B.; Mouslim, M.; Warad, I. Synthesis of Novel Cl2Co4L6 Clusterusing 1-Hydroxymethyl-3, 5-Dimethylpyrazole (LH) Ligand: Crystal Structure, Spectral, Thermal, Hirschfeld Surface Analysis and Catalytic Oxidation Evaluation. *J. Mol. Struct.* **2020**, *1199*, 126995. [CrossRef]
10. Bouroumane, N.; El Boutaybi, M.; Chetioui, S.; Bougueria, H.; Djedouani, A.; Bahari, Z.; Oussaid, A. Five Naphthalene Azo Benzene Ligands Complexed with Copper Metals: An Excellent in-Situ Catecholase Catalyst. *Mater. Today Proc.* **2021**, *45*, 7603–7607. [CrossRef]
11. Ayad, M.I. Synthesis, Characterization and Catechol Oxidase Biomimetic Catalytic Activity of Cobalt(II) and Copper(II) Complexes Containing N_2O_2 Donor Sets of Imine Ligands. *Arab. J. Chem.* **2016**, *9*, S1297–S1306. [CrossRef]
12. Mouadili, A.; El Ouafi, A.; Attayibat, A.; Radi, S.; Touzani, R. Catecholase and Tyrosinase Biomimetic Activities for Heteroatom Donor Ligands: Influence of Five Parameters. *J. Mater. Environ. Sci.* **2015**, *6*, 2166–2173.

13. Yang, L.; Lee, Y.-A.; Jung, O.-S. Unprecedented Coordination Solvate Effects of Bimetallic Copper (II) Cages on Catechol Oxidation Catalysis. *Inorg. Chem. Commun.* **2019**, *104*, 48–53. [CrossRef]
14. Ngo, K.T.; Varner, E.L.; Michael, A.C.; Weber, S.G. Monitoring Dopamine Responses to Potassium Ion and Nomifensine by In Vivo Microdialysis with Online Liquid Chromatography at One-Minute Resolution. *ACS Chem. Neurosci.* **2017**, *8*, 329–338. [CrossRef]
15. Lee, H.N.F. Scherer, and PB Messersmith. Single-molecule Mech. mussel Adhes. *Proc. Natl. Acad. Sci. USA* **2006**, *103*, 12999–13003. [CrossRef]
16. Citek, C.; Lin, B.-L.; Phelps, T.E.; Wasinger, E.C.; Stack, T.D.P. Primary Amine Stabilization of a Dicopper (III) Bis (μ-Oxo) Species: Modeling the Ligation in PMMO. *J. Am. Chem. Soc.* **2014**, *136*, 14405–14408. [CrossRef]
17. Olmedo, P.; Moreno, A.A.; Sanhueza, D.; Balic, I.; Silva-Sanzana, C.; Zepeda, B.; Verdonk, J.C.; Arriagada, C.; Meneses, C.; Campos-Vargas, R. A Catechol Oxidase AcPPO from Cherimoya (Annona Cherimola Mill.) is Localized to the Golgi Apparatus. *Plant Sci.* **2018**, *266*, 46–54. [CrossRef]
18. Mason, H.S. The Chemistry of Melanin: Vi. Mechanism of the Oxidation of Catechol by Tyrosinase. *J. Biol. Chem.* **1949**, *181*, 803–812. [CrossRef]
19. Petrik, I.D.; Davydov, R.; Ross, M.; Zhao, X.; Hoffman, B.; Lu, Y. Spectroscopic and Crystallographic Evidence for the Role of a Water-Containing H-Bond Network in Oxidase Activity of an Engineered Myoglobin. *J. Am. Chem. Soc.* **2016**, *138*, 1134–1137. [CrossRef]
20. Marion, R.; Muthusamy, G.; Geneste, F. Continuous Flow Catalysis with a Biomimetic Copper(II) Complex Covalently Immobilized on Graphite Felt. *J. Catal.* **2012**, *286*, 266–272. [CrossRef]
21. El Boutaybi, M.; Bouroumane, N.; Azzouzi, M.; Bacroume, S.; Touzani, R.; Catecholase, Z. Phenoxazinone Synthase and Copper (CuII) Complex Based on Pyrazolic Ligand: Preparation and Characterization. *Mater. Today Proc.* **2023**, 1–7. [CrossRef]
22. Misawa-Suzuki, T.; Ikeda, R.; Komatsu, R.; Toriba, R.; Miyamoto, R.; Nagao, H. Geometry and Electronic Structures of Cobalt(II) and Iron(III) Complexes Bearing Bis(2-pyridylmethyl)ether or Alkylbis(2-pyridylmethyl)amine. *Polyhedron* **2022**, *218*, 115735–115743. [CrossRef]
23. Titi, A.; Almutairi, S.; Touzani, R.; Messali, M.; Tillardd, M.; Hammouti, B.; El Kodadi, M.; Eddikee, D.; Zarrouk, A.; Warad, I. A new mixed pyrazole-diamine/Ni(II) complex, Crystal Structure, Physicochemical, Thermal and Antibacterial Investigation. *J. Mol. Struct.* **2021**, *1236*, 130304. [CrossRef]
24. Haoyu, S.Y.; He, X.; Li, S.L.; Truhlar, D.G. MN15: A Kohn–Sham global-hybrid exchange–correlation density functional with broad accuracy for multi-reference and single-reference systems and noncovalent interactions. *Chem. Sci.* **2016**, *7*, 5032–5051.
25. Badran, I.; Tighadouini, S.; Radi, S.; Zarrouk, A.; Warad, I. Experimental and first-principles study of a new hydrazine derivative for DSSC applications. *J. Mol. Struct.* **2020**, *1229*, 129799. [CrossRef]
26. Mardirossian, N.; Head-Gordon, M. Thirty years of density functional theory in computational chemistry: An overview and extensive assessment of 200 density functionals. *Mol. Phys.* **2017**, *115*, 2315–2372. [CrossRef]
27. Peverati, R.; Truhlar, D.G. Truhlar, Quest for a universal density functional: The accuracy of density functionals across a broad spectrum of databases in chemistry and physics. *Philos. Trans. R. Soc. A Math. Phys. Eng. Sci.* **2014**, *372*, 20120476. [CrossRef]
28. Goerigk, L.; Hansen, A.; Bauer, C.; Ehrlich, S.; Najibi, A.; Grimme, S. A look at the density functional theory zoo with the advanced GMTKN55 database for general main group thermochemistry, kinetics and noncovalent interactions. *PCCP* **2017**, *19*, 32184–32215. [CrossRef] [PubMed]
29. Badran, I.; Rauk, A.; Shi, Y. New Orbital Symmetry-Allowed Route for Cycloreversion of Silacyclobutane and Its Methyl Derivatives. *J. Phys. Chem. A* **2019**, *123*, 1749–1757. [CrossRef]
30. Badran, I.; Rauk, A.; Shi, Y.J. Theoretical Study on the Ring-Opening of 1,3-Disilacyclobutane and H2 Elimination. *J. Phys. Chem. A* **2012**, *116*, 11806–11816. [CrossRef]
31. Frisch, M.J.; Trucks, G.W.; Schlegel, H.B.; Scuseria, G.E.; Robb, M.A.; Cheeseman, J.R.; Scalmani, G.; Barone, V.; Petersson, G.A.; Nakatsuji, H.; et al. *Gaussian 16 Rev. C.01*; Gaussian Inc.: Wallingford, CT, USA, 2016.
32. Dennington, R.; Keith, T.; Millam, J. *GaussView, Version 5*; Semichem Inc.: Shawnee, KA, USA, 2009.
33. Hosny, N.M. Solvothermal Synthesis, Thermal and Adsorption Properties of Metal-Organic Frameworks Zn and CoZn (DPB). *J. Therm. Anal. Calorim.* **2015**, *122*, 89–95. [CrossRef]
34. Scrocco, E.; Tomasi, J. Electronic Molecular Structure, Reactivity and Intermolecular Forces: An Euristic Interpretation by Means of Electrostatic Molecular Potentials. In *Advances in Quantum Chemistry*; Elsevier: Amsterdam, The Netherlands, 1978; Volume 11, pp. 115–193.
35. Munoz-Caro, C.; Nino, A.; Senent, M.L.; Leal, J.M.; Ibeas, S. Modeling of Protonation Processes in Acetohydroxamic Acid. *J. Org. Chem.* **2000**, *65*, 405–410. [CrossRef] [PubMed]
36. El Ati, R.; Takfaoui, A.; El Kodadi, M.; Touzani, R.; Yousfi, E.B.; Almalki, F.A.; Hadda, T.B. Catechol Oxidase and Copper (I/II) Complexes Derived from Bipyrazol Ligand: Synthesis, Molecular Structure Investigation of New Biomimetic Functional Model and Mechanistic Study. *Mater. Today Proc.* **2019**, *13*, 1229–1237. [CrossRef]
37. Adam, F.; Batagarawa, M.S. Tetramethylguanidine–Silica Nanoparticles as an Efficient and Reusable Catalyst for the Synthesis of Cyclic Propylene Carbonate from Carbon Dioxide and Propylene Oxide. *Appl. Catal. A Gen.* **2013**, *454*, 164–171. [CrossRef]
38. Boyaala, R.; El Ati, R.; Khoutoul, M.; El Kodadi, M.; Touzani, R.; Hammouti, B. Biomimetic Oxidation of Catechol Employing Complexes Formed in Situ with Heterocyclic Ligands and Different Copper(II) Salts. *J. Iran. Chem. Soc.* **2018**, *15*, 85–92. [CrossRef]

39. Mouadili, A.; Abrigach, F.; Khoutoul, M.; Zarrouk, A.; Benchat, N.; Touzani, R. Biomimetic Oxidation of Catechol Employing Complexes Formed In-Situ with NH-Pyrazole Ligands and Transition Metallic Salts. *J. Chem. Pharm. Res.* **2015**, *7*, 968–979.
40. Mouadili, A.; Attayibat, A.; Radi, S.; Touzani, R. Catecholase Activity Studies of Two Multidendate Ligands Based on Pyrazole. *Arab. J. Chem. Environ. Res.* **2014**, *1*, 24–32.
41. Bedoya, J.C.; Valdez, R.; Cota, L.; Alvarez-Amparán, M.A.; Olivas, A. Performance of Al-MCM-41 Nanospheres as Catalysts for Dimethyl Ether Production. *Catal. Today* **2022**, *388*, 55–62. [CrossRef]
42. Muley, A.; Karumban, K.S.; Kumbhakar, S.; Giri, B.; Maji, S. High Phenoxazinone Synthase Activity of Two Mononuclear Cis-Dichloro Cobalt(II) Complexes with a Rigid Pyridyl Scaffold. *New J. Chem.* **2022**, *46*, 521–532. [CrossRef]
43. Kumbhakar, S.; Giri, B.; Muley, A.; Karumban, K.S.; Maji, S. Design, Synthesis, Structural, Spectral, and Redox Properties and Phenoxazinone Synthase Activity of Tripodal Pentacoordinate Mn (II) Complexes with Impressive Turnover Numbers. *Dalt. Trans.* **2021**, *50*, 16601–16612. [CrossRef]
44. Dhara, A.K.; Maity, S.; Dhar, B.B. Visible-Light-Mediated Synthesis of Substituted Phenazine and Phenoxazinone Using Eosin Y as a Photoredox Catalyst. *Org. Lett.* **2021**, *23*, 3269–3273. [CrossRef] [PubMed]
45. Khairy, M.; Mahmoud, A.H.; Khalil, K.M.S. Synthesis of Highly Crystalline $LaFeO_3$ Nanospheres for Phenoxazinone Synthase Mimicking Activity. *RSC Adv.* **2021**, *11*, 17746–17754. [CrossRef] [PubMed]
46. Chirinos, J.; Ibarra, D.; Morillo, Á.; Llovera, L.; González, T.; Zárraga, J.; Larreal, O.; Guerra, M. Synthesis, Characterization and Catecholase Biomimetic Activity of Novel Cobalt(II), Copper(II), and Iron(II) Complexes Bearing Phenylene-Bis-Benzimidazole Ligand. *Polyhedron* **2021**, *203*, 115232. [CrossRef]
47. Nehar, O.K.; Mahboub, R.; Louhibi, S.; Roisnel, T.; Aissaoui, M. New Thiosemicarbazone Schiff Base Ligands: Synthesis, Characterization, Catecholase Study and Hemolytic Activity. *J. Mol. Struct.* **2020**, *1204*, 127566–127576. [CrossRef]